



1 **Direct observations indicate photodegradable oxygenated VOCs**
2 **as larger contributors to radicals and ozone production in the**
3 **atmosphere**

4 Wenjie Wang^{1,2}, Bin Yuan^{1,3*}, Yuwen Peng^{1,3}, Hang Su^{2*}, Yafang Cheng², Suxia Yang^{1,3},
5 Caihong Wu^{1,3}, Jipeng Qi^{1,3}, Fengxia Bao², Yibo Huangfu^{1,3}, Chaomin Wang^{1,3},
6 Chenshuo Ye¹, Zelong Wang^{1,3}, Baolin Wang⁴, Xinming Wang⁵, Wei Song⁵, Weiwei
7 Hu⁵, Peng Cheng⁶, Manni Zhu^{1,3}, Junyu Zheng^{1,3}, Min Shao^{1,3}

8
9 ¹ Institute for Environmental and Climate Research, Jinan University,
10 Guangzhou 511443, China

11 ² Multiphase Chemistry Department, Max Planck Institute for Chemistry, Mainz
12 55128, Germany.

13 ³ Guangdong-Hongkong-Macau Joint Laboratory of Collaborative Innovation for
14 Environmental Quality, Guangzhou, 511443, China

15 ⁴ School of Environmental Science and Engineering, Qilu University of
16 Technology, Jinan 250353, China

17 ⁵ State Key Laboratory of Organic Geochemistry, Guangzhou Institute of
18 Geochemistry, Chinese Academy of Sciences, Guangzhou 510640, China

19 ⁶ Institute of Mass Spectrometry and Atmospheric Environment, Jinan
20 University, Guangzhou 510632, China

21
22 **Correspondence to:* Bin Yuan (byuan@jnu.edu.cn); Hang Su (h.su@mpic.de)

23
24



25 **Abstract:** Volatile organic compounds (VOCs) regulate atmospheric oxidation capacity,
26 and the reactions of VOCs are key in understanding ozone formation and its mitigation
27 strategies. When evaluating its impact, most previous studies did not fully consider the
28 role of oxygenated VOCs due to limitations of measurement technology. By using a
29 proton-transfer-reaction time-of-flight mass spectrometer (PTR-ToF-MS) combined
30 with gas chromatography mass spectrometer (GC-MS) technology, we are able to
31 quantify a large number of oxygenated VOCs in a representative urban environment in
32 southern China. Based on the new dataset, we find that non - formaldehyde (HCHO)
33 OVOCs can contribute large fractions (22-44%) of total RO_x radical production,
34 comparable or larger than the contributions from nitrous acid and formaldehyde. We
35 demonstrate that constraints using OVOCs observations are essential in modeling
36 radical and ozone production, as modelled OVOCs can be substantially lower than
37 measurements, potentially due to primary emissions and/or missing secondary sources.
38 Our results show that models without OVOC constraints using ambient measurements
39 will underestimate P(RO_x) and ozone production rate, and may also affect the
40 determination of sensitivity regime in ozone formation. Therefore, a thorough
41 quantification of photodegradable OVOCs species is in urgent need to understand
42 accurately the ozone chemistry and to develop effective control strategies.

43
44 **Keywords:** photolysis reactions; oxygenated volatile organic compounds; radical
45 production; ozone production
46



47 **1 Introduction**

48 Ground-level ozone is generated by photochemical oxidation of volatile organic
49 compounds (VOCs) under the catalysis of nitrogen oxides (NO_x) and hydroxide
50 radicals (HO_x=OH+HO₂) (Atkinson, 2000;Monks et al., 2015). In this process,
51 photolysis reactions are a crucial driving force. Photodegradable species (i.e. species
52 that is capable of photolysis) including O₃, nitrous acid (HONO), and oxygenated
53 VOCs (OVOCs) can contribute to primary production of RO_x (OH+HO₂+RO₂)
54 radicals via photolysis reactions, thereby accelerating the recycling of radicals to
55 generate ozone (Volkamer et al., 2010). The strong dependence of OH concentration
56 on j(O¹D) was found in a number of field measurements (Ehhalt and Rohrer,
57 2000;Rohrer et al., 2014b;Stone et al., 2012), implying the dominant role of
58 ultraviolet radiation and photolysis reactions in the production of HO_x radicals.
59 Edwards et al. (2014) found that the high ozone pollution in an oil and gas producing
60 basin in the U.S. in winter was caused by the photolysis of high concentrations of
61 OVOCs to generate sufficient oxidants. A recent model simulation with limited
62 OVOCs measurements by Qu et al.(Qu et al., 2021) indicated that OVOC species is
63 the largest free-radical source in the boundary layer. Another study indicated that fast
64 ozone production during winter haze episodes in China was driven by HO_x radicals
65 derived from photolysis of formaldehyde (HCHO), overcoming radical titration
66 induced by NO_x emissions (Li et al., 2021). Therefore, an accurate quantification of
67 numerous photolysis reactions is necessary to understand the mechanism of RO_x
68 radical and ozone production.

69 However, only limited number of photodegradable OVOCs species, such as
70 formaldehyde, acetaldehyde and acetone, have been measured in the field campaigns
71 in China due to the limitations of measurement technology (Lu et al., 2013;Lu et al.,
72 2012;Tan et al., 2018;Tan et al., 2019c). Many important photodegradable OVOCs,
73 such as larger aldehydes and ketones, carboxylic acids, nitrophenols, organic peroxides
74 and multifunctional species, have been rarely quantified accurately in ambient
75 environments. In such cases, the quantification of the primary production of RO_x



76 radicals induced by photolysis reactions may not be adequately accurate. Many studies
77 used photochemical models to simulate unmeasured OVOC species (Tan et al.,
78 2019b; Volkamer et al., 2010; Ling et al., 2014; Edwards et al., 2014). However, large
79 uncertainties in the simulation of OVOCs remain due to primary emissions of OVOCs
80 (McDonald et al., 2018; Karl et al., 2018; Gkatzelis et al., 2021), missing secondary
81 sources (Bloss et al., 2005; Ji et al., 2017), heterogenous uptake of aerosols and
82 unknown dilution and transmission processes (Li et al., 2014). For instance, chamber
83 experiments of the oxidation of aromatics by OH radical indicated that MCM
84 mechanism generally underestimated the formation of aldehydes, ketones and phenols
85 by 10-70% (Bloss et al., 2005; Ji et al., 2017), implying the existence of unknown
86 production pathways for these OVOC species. Furthermore, model simulations
87 frequently underestimated observed RO_x radicals in ambient studies of RO_x radicals
88 (Hofzumahaus et al., 2009; Tan et al., 2018; Lelieveld et al., 2008; Rohrer et al.,
89 2014a; Sheehy et al., 2010; Emmerson et al., 2005; Ma et al., 2019). Given that only
90 limited photodegradable OVOCs species were measured in these studies, the lack of
91 comprehensive measurements of OVOCs to constrain the model is likely to be a cause
92 of the underestimation.

93 Thus far, the concrete effects of photodegradable OVOCs on radical and ozone
94 production remains unexplored in China. Based on comprehensive field observations
95 in a mega-city in southern China, a variety of important photodegradable OVOC
96 species were measured. The contributions of these photodegradable OVOCs species
97 to the production of RO_x radicals are quantified, and the effect of photolysis reactions
98 on ozone production is quantitatively assessed.

99 **2 Materials and Methods**

100 **2.1 OVOC measurements**

101 Field measurements were conducted at an urban site in Guangzhou (113.2°E, 23°N)
102 from 14 September to 20 November 2018. The sampling site is located on the 9th floor
103 of a building on the campus of Guangzhou Institute of Geochemistry, Chinese Academy



104 of Sciences, 25 m above the ground level. This site is regarded as a typical urban site
105 in Guangzhou influenced by industrial and vehicle emissions.

106 During this campaign, an online PTR-ToF-MS (Ionicon Analytic GmbH,
107 Innsbruck, Austria) with H_3O^+ and NO^+ chemistry was used to measure ambient volatile
108 organic compounds (VOCs) (Wang et al., 2020a; Wu et al., 2020). The PTR-ToF-MS
109 automatically switches between H_3O^+ and NO^+ modes every 10-20 minutes. In each
110 mode, the background and ambient measurements were automatically switched to a
111 custom-built Platinum catalytic converter heated to 365 °C for 3 minutes to detect
112 background of the instrument. The time resolution of the measurement of PTR-ToF -
113 MS was 10 s. A total of 31 VOCs species were calibrated using either gas cylinders or
114 liquid standards. For other measured VOCs, we used the method proposed by Sekimoto
115 et al. (2017) to determine the relationship between VOC sensitivity and kinetic rate
116 constants for proton transfer reactions of H_3O^+ with VOCs. The fitted line was used to
117 determine the concentrations of those uncalibrated species. Following the discussions
118 in Sekimoto, et al. (Sekimoto et al., 2017), the uncertainties of the concentrations for
119 uncalibrated species were about 50 %. Humidity dependencies of various VOCs were
120 determined in the laboratory with absolute humidity in the range of 0–30 mmol/mol
121 (relative humidity of 0 %–92 % at 25 °C), which fully covered the humidity range
122 encountered during the entire campaign. The detailed introduction of this method has
123 been reported by Wu et al. (Wu et al., 2020).

124 Notably, PTR-ToF-MS is not capable of distinguishing isomers (Yuan et al., 2017).
125 GC-MS technique was used to measure several carbonyls that PTR-ToF-MS can not
126 distinguish, including acetaldehyde, propionaldehyde, n-butanal, n-pentanal, n-hexanal,
127 methacrolein, methyl vinyl ketone. An iodide time-of flight chemical ionization mass
128 spectrometer (ToF-CIMS) was used to measure propionic acid. Combined with the
129 measurements of GC-MS and CIMS, the isomers measured by PTR-ToF-MS can be
130 distinguished. In OVOC species, hydroxyacetone and propionic acid ($\text{C}_3\text{H}_6\text{O}_2$), acetone
131 and propanal ($\text{C}_3\text{H}_6\text{O}$), methyl ethyl ketone and butanal ($\text{C}_4\text{H}_8\text{O}$), MVK and MACR
132 ($\text{C}_4\text{H}_6\text{O}$) are all isomers. The average concentration of propionic acid measured by
133 CIMS was 0.23 ppb, significantly lower than that of the concentration of $\text{C}_3\text{H}_6\text{O}_2$



134 measured by PTR-ToF-MS (~1.5 ppb). The hydroxyacetone concentrations were
135 determined by the difference between PTR-ToF-MS and CIMS measurements.
136 Meanwhile, the concentration of propionaldehyde (average of 0.35 ppb) and n-butanal
137 (average of 0.17 ppb) measured by GC-MS were also respectively far lower than the
138 concentration of C₃H₆O (average of 4.4 ppb) and C₄H₈O (average of 1.8 ppb) measured
139 by PTR-ToF-MS. The concentrations of acetone and methyl ethyl ketone were
140 determined by the difference between PTR-ToF-MS and GC-MS measurements. The
141 concentrations of MVK and MACR were determined according to C₄H₆O
142 concentration measured by PTR-ToF-MS and the ratio of MVK to MACR measured by
143 GC-MS. Additionally, the concentration of CH₄O₂ and CH₄O₃ were also quantified,
144 which were tentatively attributed to methyl hydroperoxide (CH₃OOH) and
145 hydroxymethyl hydroperoxide (HOCH₂OOH), respectively. Additionally, we also
146 measured concentrations of several small carbon-number acids, including formic acid,
147 acetic acid, and propionic acid (**Figure S1**). However, the photolysis wavelength bands
148 of these species are all less than 260 nm. Given the sunlight that can reach the ground
149 is generally greater than 290 nm, these small carbon-number acids cannot photolyze
150 significantly near the ground. An exception is pyruvic acid which is also a small carbon-
151 number acid but with a wide photolysis band that can reach 460 nm because of its
152 carbonyl functional group (Horowitz et al., 2001; Mellouki and Mu, 2003; Berges and
153 Warneck, 1992). Therefore, the photolysis of pyruvic acid was included in the analysis
154 as it can significantly contribute to the production of RO_x radicals.

155 In addition to the specific species mentioned above, PTR-ToF-MS measured
156 carbonyls with higher carbon number including C_nH_{2n}O (n>5), C_nH_{2n-2}O (n>3), C_nH_{2n-2}
157 O₂ (n>3), C_nH_{2n-4}O₂ (n>3) and C_nH_{2n-4}O₃ (n>3). Apparently, multiple isomers that
158 can't be distinguished specifically may contribute to these species. The measured
159 photodegradable OVOCs species and their concentrations are summarized in **Table S1**.

160 2.2 Other measurements

161 HONO was measured by a custom-built LOPAP (LONg Path Absorption
162 Photometer) based on wet chemical sampling and photometric detection (Yu et al.,



2021). HCHO was measured by a custom-built instrument based on the Hantzsch
reaction and absorption photometry. Total OH reactivity was measured by the
comparative reactivity method (CRM) (Sinha et al., 2008; Wang et al., 2021). In this
method, pyrrole (C₄H₅N) was used as the reference substance and was quantified by a
quadrupole PTR-MS (Ionicon Analytic, Austria). Non-methane hydrocarbons
(NMHCs) were measured using a gas chromatography-mass spectrometer/flame
ionization detector (GC-MS/FID) system, coupled with a cryogen-free pre-
concentration device. Nitrogen oxides (NO_x= NO + NO₂), ozone (O₃), sulfur dioxide
(SO₂) and carbon monoxide (CO) were measured by NO_x analyzer (Thermo
Scientific, Model 42i), O₃ analyzer (Thermo Scientific, 150 Model 49i), SO₂ analyzer
(Thermo Scientific, Model 43i) and CO analyzer (Thermo Scientific, Model 48i). The
meteorological data, including temperature (T), relative humidity (RH) and wind
speed and direction (WS, WD) were recorded by Vantage Pro2 Weather Station
(Davis Instruments Inc., Vantage Pro2) with the time resolution of 1 min. Photolysis
frequencies including j(HONO), j(NO₂), j(H₂O₂), j(HCHO) and j(O¹D) were
measured by a spectrometer (Focused Photonics Inc., PFS-100).

2.3 Observation-based box model

A zero-dimensional box model coupled with the Master Chemical Mechanism
(MCM) v3.3.1 chemical mechanism (Jenkin et al., 2003; Saunders et al., 2003) was used
to simulate RO_x production and losses, and O₃ production rates during the field
campaign. The model simulation was constrained to the observations of meteorological
parameters, photolysis frequencies, and concentrations of non-methane hydrocarbons
(NMHCs), OVOCs, NO, NO₂, O₃, CO, SO₂ and nitrous acid (HONO). All constraints
were averaged to generate a synchronized 1-h time resolution dataset. The model runs
were performed in a time-dependent mode with spin-up of two days. A 24-h lifetime
was introduced for all simulated species, including secondary species and radicals, to
approximately simulate dry deposition and other losses of these species (Lu et al.,
2013; Wang et al., 2020b). This lifetime corresponds to an assumed deposition velocity
of 1.2 cm s⁻¹ and a well-mixed boundary layer height of about 1 km. Sensitivity tests



192 show that this assumed deposition lifetime has a relatively small influence on the
193 reactivity of modeled oxidation products, RO_x radicals and ozone production rates. The
194 ozone production rate (P(O₃)) were calculated according to E1:

$$195 \quad P(O_3) = k_{HO_2+NO}[HO_2][NO] + \sum_i(k_{RO_2+NO}^i [RO_2^i][NO]) \quad E1$$

196 The production rate of RO_x radicals (P(RO_x)) is equal to the sum of the rates at
197 which all photodegradable species generate RO_x radicals through the photolysis
198 reactions, as shown in E2.

$$199 \quad P(RO_x) = 2 \times [O_3] \times j(O^1D) \times \theta + [HONO] \times j(HONO) + \sum_i[OVOC_i] \times j_i \times k_i \quad E2$$

200 where θ is the fraction of O¹D from ozone photolysis that reacts with water vapor.
201 OVOC_i represents each OVOCs species, j_i represents the photolysis frequency of each
202 OVOC species, and k_i represents the number of RO_x radical generated from the
203 photolysis of each OVOC molecule. For most OVOCs species, k_i is equal to 2.

204 The photolysis frequencies of measured photodegradable species were calculated
205 based on measured actinic flux combined with absorption cross sections and
206 photolysis quantum yields reported in Jet Propulsion Laboratory (JPL) publication
207 (Burkholder et al., 2020). However, absorption cross sections and photolysis quantum
208 yields for nitrophenol and methyl nitrophenol are unavailable from JPL publication.
209 Yuan et al. (2016) have reported that photolysis was the most efficient loss pathway
210 for nitrophenol in the gas phase. Different values of absorption cross sections and
211 quantum yields for nitrophenol have been reported (Chen et al., 2011; Sangwan and
212 Zhu, 2018; Bejan et al., 2006). In this study, we used the values from Chen et al. (Chen
213 et al., 2011), which can reproduce well the observed concentrations of nitrophenol and
214 methyl nitrophenol during the measurement period.

215 Absorption cross sections and quantum yields are not available for carbonyls
216 with large carbon number, and absorption cross sections and quantum yields of
217 species with similar structure are used as a surrogate, following the method described
218 in Jenkin et al., (1997) (Jenkin et al., 1997) (e.g. C₂H₅C(O)CH₃ is used as a surrogate
219 for aliphatic ketones with more carbons). Another issue is that carbonyls with large
220 carbon number (C_nH_{2n}O, n>5; C_nH_{2n-2}O, n>3; C_nH_{2n-2}O₂, n>3; C_nH_{2n-4}O₂, n>3; C_nH_{2n-}
221 4O₃, n>3) measured by PTR-ToF-MS may include contributions from multiple



222 isomers, and the fraction of each individual species cannot be obtained. Hence, each
223 molecular formula corresponds to multiple molecular structures and thus corresponds
224 to multiple photolysis frequencies. Here, we calculate the $P(\text{RO}_x)$ of these species in
225 two scenarios: (1) each molecular formula corresponds to minimum photolysis
226 frequency of all potential species (e.g. aliphatic ketones); (2) each molecular formula
227 corresponds to maximum photolysis frequency of all potential species (e.g.
228 aldehydes). As a result, photolysis frequencies of these carbonyls with large carbon
229 number were assigned to the ranges of $1.2 \times 10^{-6} \sim 6.5 \times 10^{-6}$, $1.2 \times 10^{-6} \sim 6.5 \times 10^{-6}$, 1.2×10^{-6}
230 $\sim 1.2 \times 10^{-4}$, $1.2 \times 10^{-6} \sim 3.0 \times 10^{-4}$ and $1.2 \times 10^{-6} \sim 1.8 \times 10^{-4} \text{ s}^{-1}$, respectively (Jenkin et al.,
231 1997) (**Table S1**). The lowest and highest values of these photolysis frequencies were
232 separately used to determine the lower and upper limits of $P(\text{RO}_x)$. Therefore, the
233 total $P(\text{RO}_x)$ contributed by all these OVOC species could be investigated.

234 **3 Results and discussion**

235 **3.1 Overview of the observations**

236 During the observation period, we used PTR-ToF-MS and GC-MS technology to
237 measure more than 20 photodegradable OVOCs species. The concentrations and
238 photolysis frequencies of measured photodegradable OVOCs species are summarized
239 in **Table S1** and **Figure 1**. Previous studies have reported that these species have
240 relatively large absorption cross section and quantum yield (Burkholder et al., 2020).
241 The measured daytime average photolysis frequencies for these species were generally
242 larger than $1.3 \times 10^{-6} \text{ s}^{-1}$.

243 **Figure 1** presents the average diurnal variation of photodegradable OVOCs
244 species during the measurement period. The concentrations of these species ranged
245 from 0.01 to 10 ppb. HCHO, methylglyoxal, propionaldehyde, n-butanal, n-pentanal,
246 MVK+MACR, pyruvic acid, formic acid, acetic acid, and CH_3OOH had similar diurnal
247 variation patterns. The concentrations of these species started to increase from about
248 6:00 in the morning, and peaked at 13:00-16:00, after which the concentrations
249 gradually decreased. This diurnal variation pattern is a typical secondary production



250 pattern, and thus we deduce that these species primarily came from secondary
251 production. Acetaldehyde, acetone and acrolein showed diurnal variations without
252 significant variations throughout the day, as these species were contributed by both
253 secondary generation and primary emissions or background contribution (Wu et al.,
254 2020). It is notable that acrolein, nitrophenol and methylnitrophenol all peaked at 20:00
255 in the evening, which is likely due to primary emissions e.g. biomass burning (Ye et al.,
256 2021).

257 The ratio of secondary OVOCs to NMHCs can characterize the degree of the
258 conversion of emitted NMHC to secondary OVOCs through oxidation reactions.
259 **Figure S2** presents the correlation between daily daytime average of HCHO (and
260 pyruvic acid) concentration versus OH reactivity from hydrocarbons, i.e.,
261 HCHO/ k_{OH_NMHC} ratio (and pyruvic acid/ k_{OH_NMHC} ratio) and $j(\text{NO}_2)$. Both
262 HCHO/ k_{OH_NMHC} and pyruvic acid/ k_{OH_NMHC} ratios displayed significant positive
263 correlation with $j(\text{NO}_2)$. These results suggest that the enhancement of the photolysis
264 rates converted more NMHCs into secondary OVOCs, suggesting the crucial role of
265 photolysis reactions in the air mass aging and the occurrence of secondary pollution.

266 **3.2 Contribution of photolysis reactions to the production of RO_x radicals**

267 The photolysis of O₃, HONO and OVOCs are the most important contributors to
268 the production of RO_x radicals. All observed photodegradable species, including O₃,
269 HONO and OVOCs, were constrained in the box model to calculate P(RO_x). The
270 calculated P(RO_x) was basically determined by concentrations of these observed
271 photodegradable species. Using the possible ranges of photolysis frequencies of
272 carbonyls with more carbon number that are not possible to assign into specific
273 individual species, we can obtain the possible widest variation range of P(RO_x). As
274 shown in **Figure 2a**, the minimum (solid line) and maximum (dashed line) of P(RO_x)
275 calculated during the campaign peaked at 3.6 ppb h⁻¹ and 5.4 ppb h⁻¹, respectively. The
276 P(RO_x) determined in this study is very close to those reported in the Autumn 2014 in
277 Pearl River Delta with peak values of 3 ~ 4 ppb h⁻¹ (Tan et al., 2019a) and the summer
278 2014 in Wangdu, Hebei (peak value of 5 ppb h⁻¹) (Tan et al., 2017), and lower than



279 those in the summer 2006 in Beijing (peak value of about 7 ppb h⁻¹) (Lu et al., 2013)
280 and the summer 2006 in Guangzhou (peak value of about 10 ppb h⁻¹) (Lu et al., 2012),
281 and higher than those in the winter of 2016 in Beijing (peak value of about 1 ppb h⁻¹)
282 (Tan et al., 2018) and the winter in the oil and gas basin of Utah, USA (daytime average
283 value of 0.77 ppb h⁻¹) (Edwards et al., 2014). Note that these previous studies mentioned
284 above usually only measured a few simple carbonyls such as HCHO, acetaldehyde and
285 acetone and the P(RO_x) contributed by photolysis of other OVOCs was calculated by
286 model simulations, which may lead to large uncertainties.

287 For the scenario of minimum OVOCs contribution, HONO contributed the most
288 to P(RO_x) (37%), followed by O₃ (20%) and HCHO (21%). The contribution of non-
289 HCHO OVOCs was 22% (**Figure 2a**). For the scenario of maximum OVOCs
290 contribution, the contribution of non-HCHO OVOCs increased to 44%. In total,
291 OVOCs contributed 43% ~ 59% of P(RO_x), which was higher than the contribution of
292 HONO. This is different from previous studies reporting HONO contributed more to
293 P(RO_x) than OVOCs in China (Tan et al., 2019a; Tan et al., 2017; Tan et al., 2018; Tan
294 et al., 2019b). Nevertheless, it is notable that the contributions of HONO to P(RO_x) in
295 the early morning were higher than those of OVOCs due to the accumulation of HONO
296 in nighttime, while OVOCs dominate P(RO_x) at noon when photochemistry was most
297 active (**Figure 2a**). Furthermore, previous studies in China indicated that HCHO was
298 the dominant contributor to P(RO_x) among OVOC species and the contributions of
299 other OVOC species was generally smaller than that of HCHO (Tan et al., 2019a; Tan
300 et al., 2017; Tan et al., 2018; Tan et al., 2019b). In contrast, the results of this study
301 suggest that non-HCHO OVOCs have a potential to be a larger contributor than HCHO
302 and HONO, revealing the importance of non-HCHO OVOCs in radical production. The
303 difference between this study and previous studies in China is primarily attributed to
304 more OVOC species measured in this study than previous studies. Nevertheless, the
305 existing isomers of carbonyls with more carbons lead to large uncertainties in the
306 quantification of P(RO_x) as shown in **Figure 2a**. Therefore, precise distinction of these
307 isomers in the future is crucial to accurately quantify P(RO_x). In addition, absorption
308 cross-section and quantum yield of many photodegradable OVOC species with large



309 carbon numbers, especially multifunctional species, are not experimentally determined.
310 As a result, the photolysis frequencies of these species are not available, which also
311 leads to uncertainties in quantifying $P(\text{RO}_x)$. As measurements of many organic
312 compounds may not be possible at least in the near future, construction of
313 parameterization method for photolysis frequencies of oxygenated VOCs either based
314 on chemical formula or functional groups at isomeric level will help to reduce this
315 uncertainty in the future.

316 As a comparison with the observation-determined $P(\text{RO}_x)$, $P(\text{RO}_x)$ was also
317 simulated by the box model without all observed OVOC species constrained. As shown
318 in **Figure 3a**, the simulation of the box model without all observed OVOC species
319 constrained underestimated $P(\text{RO}_x)$ significantly compared to observation-determined
320 $P(\text{RO}_x)$. The underestimation of $P(\text{RO}_x)$ was 16% and 44% when using the lower and
321 higher limits of OVOCs photolysis frequencies, respectively (red solid line and red
322 dashed line in **Figure 3a**). The underestimation of $P(\text{RO}_x)$ was due to the
323 underestimation of photodegradable OVOCs simulated by the photochemical model
324 (**Table S2**). In general, most photodegradable OVOCs were underestimated by 10~100%
325 by box model except for MVK and MACR. The underestimation of photodegradable
326 OVOCs can be caused by missing primary emissions (McDonald et al., 2018;Karl et
327 al., 2018;Gkatzelis et al., 2021) or unknown secondary source of these OVOCs species
328 (Bloss et al., 2005;Ji et al., 2017). Direct flux measurements of VOCs based on the eddy
329 covariance technique showed that the contribution of typical urban emission sources
330 comprised of a surprisingly large portion of OVOCs (Karl et al., 2018). In addition,
331 some experimental studies indicated that MCM mechanism generally underestimated
332 formation of aldehydes, ketones and phenols from the oxidation of aromatics by OH
333 radical (Bloss et al., 2005;Ji et al., 2017), suggesting the existence of unknown
334 secondary source of these OVOCs species. This evidence suggests that it is essential to
335 use ambient measurements of OVOCs as constraints in models at least until primary
336 and secondary sources of OVOCs are better understood.

337 Previous studies in Pearl River Delta and North China Plain of China found that
338 photochemical models significantly underestimated measured concentrations of OH



339 radicals, indicating the existence of unknown sources of RO_x radicals in the atmosphere
340 (Lu et al., 2012; Lu et al., 2013; Tan et al., 2019c; Hofzumahaus et al., 2009; Ma et al.,
341 2019). For instance, comprehensive measurements in winter in Beijing showed that the
342 photochemical box model greatly underestimated OH, HO₂ and RO₂ radicals by 50%
343 ~ 12 fold during the pollution periods (Tan et al., 2018; Ma et al., 2019). Through the
344 budget analysis of the source and sink of radicals, the researchers believed that the
345 missing P(RO_x) was the primary cause of the underestimation of HO₂ and RO₂
346 concentrations (Tan et al., 2018). Given that most photodegradable OVOCs were not
347 constrained in box model used in these previous studies of RO_x radicals, the results of
348 our study provide a direction for solving this issue regarding underestimated RO_x
349 radical concentrations. Therefore, it is imperative to continuously improve
350 measurement technologies to achieve accurate quantification of more photodegradable
351 OVOC species, thereby improving our understanding of the issues with respect to the
352 closure of RO_x radicals in the atmosphere.

353 **3.3 The role of photolysis reactions in ozone pollution**

354 The box model was used to evaluate the effect of the photodegradable OVOCs
355 species on ozone production rate during the whole campaign. P(O₃) were simulated
356 with and without all of measured photodegradable OVOCs species constrained in the
357 box model, respectively. As shown in **Figure 3b**, compared to the scenario with
358 observed photodegradable OVOCs species constrained in box model, the scenario
359 without constraining OVOCs underestimated peak value of P(O₃) by 15~38%. The
360 underestimation of P(O₃) was due to the underestimation of OVOCs by the box model
361 (**Table S2**). As shown in **Figure 4**, the dependence of daily peak O₃ concentrations on
362 NO_x concentrations was calculated by the box model with and without all of
363 measured photodegradable OVOCs species constrained. The NO_x concentration level
364 corresponding to maximum of ozone concentration (NO_x (O₃ max)) was determined. In
365 reality, this NO_x concentration level is the threshold to distinguish between VOC-
366 limited and NO_x-limited regimes (Edwards et al., 2014; Womack et al., 2019). Ozone
367 production is NO_x-limited if the ambient NO_x concentration is lower than the



368 threshold of NO_x, but is in VOC-limited regime if ambient NO_x concentration higher
369 than the threshold of NO_x. The larger threshold of NO_x represents higher possibility
370 of ozone production in NO_x limited regime. The threshold of NO_x for the scenario
371 with observed photodegradable OVOCs species constrained is 21%~52% higher than
372 that without observed photodegradable OVOCs species constrained (**Figure 4**). This
373 suggests that the box model simulation without constraining OVOCs will
374 overestimate the VOC-limited degree due to the underestimation of OVOCs, and thus
375 overestimate the effect of VOCs reduction in reducing ozone pollution, which in turn
376 may not determine the ozone control strategy correctly. Therefore, it is necessary to
377 constrain these important photodegradable species in photochemical models to
378 calculate P(O₃) level and to diagnose ozone sensitivity regimes accurately.

379 O₃ production rate can be expressed as the product of P(RO_x) and radical chain
380 length (ChL) as shown in E3 (Tonnesen and Dennis, 2000).

$$381 \quad P(O_3) = P(RO_x) \times \frac{\text{Rate}(HO_2+NO) + \text{Rate}(RO_2+NO)}{P(RO_x)} = P(RO_x) \times ChL \quad E3$$

382 where Rate (HO₂+NO) and Rate (RO₂+NO) represent the reaction rates between
383 HO₂ and NO and between RO₂ and NO, respectively.

384 Two ozone pollution episodes (from 19 September to 27 September and from 30
385 September to 9 October, respectively) were identified during the campaign from 14
386 September to 20 November 2018 (**Figure S3, Table S3**). The temporal variations of
387 P(O₃) and P(RO_x) overall showed good consistency with those of ozone concentrations
388 (**Figure S4**). P(O₃) and P(RO_x) in the two ozone pollution episodes are higher than
389 those in the non-pollution period (**Figure 5, Figure S5**). ChL levels were similar
390 between the ozone pollution episodes and the non-pollution period (**Figure S5**).
391 Therefore, the substantial increase of P(RO_x) in the ozone pollution episode played a
392 crucial role in the accelerated ozone production. Furthermore, the ratio of P(RO_x) from
393 OVOCs photolysis to total P(RO_x) in the two ozone pollution episodes is higher than
394 that in the non-pollution period, denoting higher contribution of OVOCs photolysis to
395 P(RO_x) in the ozone pollution episodes (**Figure 5**). These results indicate that the
396 accelerating production of OVOCs had a significant positive feedback effect on ozone



397 pollution. This is broadly consistent with the wintertime observations in an oil and gas
398 basin in Utah, USA, which found that a very high VOC to NO_x ratio optimized
399 production of secondary OVOCs, leading to OVOC photolysis as a dominant oxidant
400 source (Edwards et al., 2014).

401 **4 Summary and Conclusion**

402 In summary, comprehensive measurements of photodegradable species advance
403 our understand of radical sources and ozone production in an urban environment. By
404 using PTR-ToF-MS in a representative urban environment, a large number of
405 photodegradable OVOCs were measured. These measurements make it possible to
406 directly quantify their contribution to RO_x radical production. We found that non-
407 HCHO OVOCs can be a larger contributor to P(RO_x) than HCHO and HONO.
408 Photochemical models without constrained OVOC species will significantly
409 underestimate P(RO_x) and ozone production rates and overestimate the effect of VOCs
410 reduction in reducing ozone pollution. Therefore, it is important to measure these
411 photodegradable species and use these observations as constraints to better quantify
412 radical and ozone production.

413 Thanks to the improvement of technology in the recent years, large number of
414 OVOCs species in the atmosphere can be measured by the emerging online chemical
415 ionization mass spectrometers, including PTR-ToF-MS and CIMS. However,
416 photolysis frequencies of these OVOCs species, especially those with multiple
417 functional groups, are still not available or difficult to quantify using current existing
418 information, which poses large uncertainties in the quantification of P(RO_x) and ozone
419 production. Hence, more laboratory studies on photolysis of organic compounds, better
420 parameterization of photolysis frequencies using chemical formula/functional groups,
421 and measurements of oxygenated VOCs at isomeric level will help to decrease this
422 uncertainty in the future.

423



424 **Data availability**

425 The observational data used in this study are available from corresponding authors
426 upon request (byuan@jnu.edu.cn)

427 **Author contributions**

428 BY, WJW and HS designed the research. WJW and BY prepared the manuscript
429 with contributions from other authors. WJW performed data analysis with contributions
430 from YWP, YFC, SXY and FXB. CHW, JPQ, YBH, CMW, CSY, ZLW, BLW, XMW,
431 WS, WWH, PC, MNZ, JYZ, and MS collected data

432 **Competing interests**

433 The authors declare that they have no known competing financial interests or personal
434 relationships that could have appeared to influence the work reported in this paper.

435

436 **Acknowledgements**

437 This work was supported by the National Key R&D Plan of China (grant No.
438 2019YFE0106300), the National Natural Science Foundation of China (grant No.
439 41877302, 41905111), Guangdong Natural Science Funds for Distinguished Young
440 Scholar (grant No. 2018B030306037), Key-Area Research and Development Program
441 of Guangdong Province (grant No. 2019B110206001), Guangdong Soft Science
442 Research Program (grant No. 2019B101001005), and Guangdong Innovative and
443 Entrepreneurial Research Team Program (grant No. 2016ZT06N263). This work was
444 also supported by Special Fund Project for Science and Technology Innovation Strategy
445 of Guangdong Province (Grant No.2019B121205004).

446



447 **References:**

- 448 Atkinson, R.: Atmospheric chemistry of VOCs and NO_x, *Atmos. Environ.*, 34, 2063-
449 2101, 2000.
- 450 Bejan, I., Abd El Aal, Y., Barnes, I., Benter, T., Bohn, B., Wiesen, P., and Kleffmann, J.:
451 The photolysis of ortho-nitrophenols: a new gas phase source of HONO, *Physical*
452 *Chemistry Chemical Physics*, 8, 2028-2035, 2006.
- 453 Berges, M. G., and Warneck, P.: Product quantum yields for the 350 nm
454 photodecomposition of pyruvic acid in air, *Berichte der Bunsengesellschaft für*
455 *physikalische Chemie*, 96, 413-416, 1992.
- 456 Bloss, C., Wagner, V., Bonzanini, A., Jenkin, M. E., Wirtz, K., Martin-Reviejo, M., and
457 Pilling, M. J.: Evaluation of detailed aromatic mechanisms (MCMv3 and MCMv3.1)
458 against environmental chamber data, *Atmos. Chem. Phys.*, 5, 623-639, 10.5194/acp-5-
459 623-2005, 2005.
- 460 Burkholder, J., Sander, S., Abbatt, J., Barker, J., Cappa, C., Crouse, J., Dibble, T., Huie,
461 R., Kolb, C., and Kurylo, M.: Chemical kinetics and photochemical data for use in
462 atmospheric studies; evaluation number 19, Pasadena, CA: Jet Propulsion Laboratory,
463 National Aeronautics and Space ..., 2020.
- 464 Chen, J., Wenger, J. C., and Venables, D. S.: Near-ultraviolet absorption cross sections
465 of nitrophenols and their potential influence on tropospheric oxidation capacity, *The*
466 *Journal of Physical Chemistry A*, 115, 12235-12242, 2011.
- 467 Edwards, P. M., Brown, S. S., Roberts, J. M., Ahmadov, R., Banta, R. M., deGouw, J.
468 A., Dubé, W. P., Field, R. A., Flynn, J. H., Gilman, J. B., Graus, M., Helmig, D., Koss,
469 A., Langford, A. O., Lefter, B. L., Lerner, B. M., Li, R., Li, S.-M., McKeen, S. A.,
470 Murphy, S. M., Parrish, D. D., Senff, C. J., Soltis, J., Stutz, J., Sweeney, C., Thompson,
471 C. R., Trainer, M. K., Tsai, C., Veres, P. R., Washenfelder, R. A., Warneke, C., Wild, R.
472 J., Young, C. J., Yuan, B., and Zamora, R.: High winter ozone pollution from carbonyl
473 photolysis in an oil and gas basin, *Nature*, 514, 351-354, 10.1038/nature13767, 2014.
- 474 Ehhalt, D. H., and Rohrer, F.: Dependence of the OH concentration on solar UV, *J.*
475 *Geophys. Res.-Atmos.*, 105, 3565-3571, 10.1029/1999jd901070, 2000.
- 476 Emmerson, K. M., Carslaw, N., Carpenter, L. J., Heard, D. E., Lee, J. D., and Pilling,
477 M. J.: Urban Atmospheric Chemistry During the PUMA Campaign 1: Comparison of
478 Modelled OH and HO₂ Concentrations with Measurements, *Journal of Atmospheric*
479 *Chemistry*, 52, 143-164, 10.1007/s10874-005-1322-3, 2005.
- 480 Gkatzelis, G. I., Coggon, M. M., McDonald, B. C., Peischl, J., Gilman, J. B., Aikin, K.
481 C., Robinson, M. A., Canonaco, F., Prevot, A. S., and Trainer, M.: Observations confirm
482 that volatile chemical products are a major source of petrochemical emissions in US
483 cities, *Environmental science & technology*, 55, 4332-4343, 2021.
- 484 Hofzumahaus, A., Rohrer, F., Lu, K., Bohn, B., Brauers, T., Chang, C.-C., Fuchs, H.,
485 Holland, F., Kita, K., and Kondo, Y.: Amplified trace gas removal in the troposphere,
486 *Science*, 324, 1702-1704, 2009.
- 487 Horowitz, A., Meller, R., and Moortgat, G. K.: The UV-VIS absorption cross sections
488 of the α -dicarbonyl compounds: pyruvic acid, biacetyl and glyoxal, *Journal of*
489 *Photochemistry and Photobiology A: Chemistry*, 146, 19-27, 2001.



- 490 Jenkin, M. E., Saunders, S. M., and Pilling, M. J.: The tropospheric degradation of
491 volatile organic compounds: a protocol for mechanism development, *Atmos. Environ.*,
492 31, 81-104, 1997.
- 493 Jenkin, M. E., Saunders, S. M., Wagner, V., and Pilling, M. J.: Protocol for the
494 development of the Master Chemical Mechanism, MCM v3 (Part B): tropospheric
495 degradation of aromatic volatile organic compounds, *Atmospheric Chemistry and*
496 *Physics*, 3, 181-193, 10.5194/acp-3-181-2003, 2003.
- 497 Ji, Y., Zhao, J., Terazono, H., Misawa, K., Levitt, N. P., Li, Y., Lin, Y., Peng, J., Wang,
498 Y., Duan, L., Pan, B., Zhang, F., Feng, X., An, T., Marrero-Ortiz, W., Secret, J., Zhang,
499 A. L., Shibuya, K., Molina, M. J., and Zhang, R.: Reassessing the atmospheric oxidation
500 mechanism of toluene, *Proceedings of the National Academy of Sciences*, 114, 8169-
501 8174, 10.1073/pnas.1705463114, 2017.
- 502 Karl, T., Striednig, M., Graus, M., Hammerle, A., and Wohlfahrt, G.: Urban flux
503 measurements reveal a large pool of oxygenated volatile organic compound emissions,
504 *Proceedings of the National Academy of Sciences*, 115, 1186-1191, 2018.
- 505 Lelieveld, J., Butler, T. M., Crowley, J. N., Dillon, T. J., Fischer, H., Ganzeveld, L.,
506 Harder, H., Lawrence, M. G., Martinez, M., Taraborrelli, D., and Williams, J.:
507 Atmospheric oxidation capacity sustained by a tropical forest, *Nature*, 452, 737-740,
508 10.1038/nature06870, 2008.
- 509 Li, K., Jacob, D. J., Liao, H., Qiu, Y., Shen, L., Zhai, S., Bates, K. H., Sulprizio, M. P.,
510 Song, S., and Lu, X.: Ozone pollution in the North China Plain spreading into the late-
511 winter haze season, *Proceedings of the National Academy of Sciences*, 118, 2021.
- 512 Li, X., Rohrer, F., Brauers, T., Hofzumahaus, A., Lu, K., Shao, M., Zhang, Y. H., and
513 Wahner, A.: Modeling of HCHO and CHOCHO at a semi-rural site in southern China
514 during the PRIDE-PRD2006 campaign, *Atmos. Chem. Phys.*, 14, 12291-12305,
515 10.5194/acp-14-12291-2014, 2014.
- 516 Ling, Z., Guo, H., Lam, S., Saunders, S., and Wang, T.: Atmospheric photochemical
517 reactivity and ozone production at two sites in Hong Kong: Application of a master
518 chemical mechanism-photochemical box model, *Journal of Geophysical Research:*
519 *Atmospheres*, 119, 10567-10582, 2014.
- 520 Lu, K., Rohrer, F., Holland, F., Fuchs, H., Bohn, B., Brauers, T., Chang, C., Häsel, R.,
521 Hu, M., and Kita, K.: Observation and modelling of OH and HO₂ concentrations in the
522 Pearl River Delta 2006: a missing OH source in a VOC rich atmosphere, *Atmospheric*
523 *chemistry and physics*, 12, 1541, 2012.
- 524 Lu, K. D., Hofzumahaus, A., Holland, F., Bohn, B., Brauers, T., Fuchs, H., Hu, M.,
525 Haseler, R., Kita, K., Kondo, Y., Li, X., Lou, S. R., Oebel, A., Shao, M., Zeng, L. M.,
526 Wahner, A., Zhu, T., Zhang, Y. H., and Rohrer, F.: Missing OH source in a suburban
527 environment near Beijing: observed and modelled OH and HO₂ concentrations in
528 summer 2006, *Atmospheric Chemistry and Physics*, 13, 1057-1080, 10.5194/acp-13-
529 1057-2013, 2013.
- 530 Ma, X., Tan, Z., Lu, K., Yang, X., Liu, Y., Li, S., Li, X., Chen, S., Novelli, A., and Cho,
531 C.: Winter photochemistry in Beijing: Observation and model simulation of OH and
532 HO₂ radicals at an urban site, *Science of the Total Environment*, 685, 85-95, 2019.
- 533 McDonald, B. C., De Gouw, J. A., Gilman, J. B., Jathar, S. H., Akherati, A., Cappa, C.



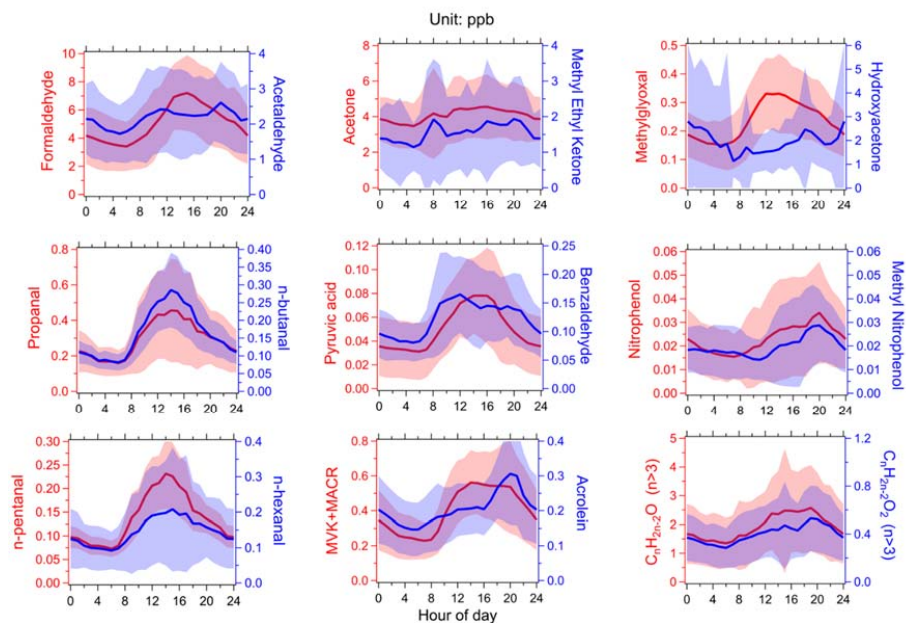
- 534 D., Jimenez, J. L., Lee-Taylor, J., Hayes, P. L., and McKeen, S. A.: Volatile chemical
535 products emerging as largest petrochemical source of urban organic emissions, *Science*,
536 359, 760-764, 2018.
- 537 Mellouki, A., and Mu, Y.: On the atmospheric degradation of pyruvic acid in the gas
538 phase, *Journal of Photochemistry and Photobiology A: Chemistry*, 157, 295-300, 2003.
- 539 Monks, P. S., Archibald, A., Colette, A., Cooper, O., Coyle, M., Derwent, R., Fowler,
540 D., Granier, C., Law, K. S., and Mills, G.: Tropospheric ozone and its precursors from
541 the urban to the global scale from air quality to short-lived climate forcer, *Atmospheric
542 Chemistry and Physics*, 15, 8889-8973, 2015.
- 543 Qu, H., Wang, Y., Zhang, R., Liu, X., Huey, L. G., Sjostedt, S., Zeng, L., Lu, K., Wu,
544 Y., and Shao, M.: Chemical Production of Oxygenated Volatile Organic Compounds
545 Strongly Enhances Boundary-Layer Oxidation Chemistry and Ozone Production,
546 *Environmental Science & Technology*, 2021.
- 547 Rohrer, F., Lu, K., Hofzumahaus, A., Bohn, B., Brauers, T., Chang, C.-C., Fuchs, H.,
548 Häsel, R., Holland, F., and Hu, M.: Maximum efficiency in the hydroxyl-radical-
549 based self-cleansing of the troposphere, *Nature Geoscience*, 7, 559-563, 2014a.
- 550 Rohrer, F., Lu, K., Hofzumahaus, A., Bohn, B., Brauers, T., Chang, C.-C., Fuchs, H.,
551 Häsel, R., Holland, F., Hu, M., Kita, K., Kondo, Y., Li, X., Lou, S., Oebel, A., Shao,
552 M., Zeng, L., Zhu, T., Zhang, Y., and Wahner, A.: Maximum efficiency in the hydroxyl-
553 radical-based self-cleansing of the troposphere, *Nature Geoscience*, 7, 559-563,
554 10.1038/ngeo2199, 2014b.
- 555 Sangwan, M., and Zhu, L.: Role of methyl-2-nitrophenol photolysis as a potential
556 source of OH radicals in the polluted atmosphere: implications from laboratory
557 investigation, *The Journal of Physical Chemistry A*, 122, 1861-1872, 2018.
- 558 Saunders, S. M., Jenkin, M. E., Derwent, R., and Pilling, M.: Protocol for the
559 development of the Master Chemical Mechanism, MCM v3 (Part A): tropospheric
560 degradation of non-aromatic volatile organic compounds, 2003.
- 561 Sekimoto, K., Li, S.-M., Yuan, B., Koss, A., Coggon, M., Warneke, C., and de Gouw,
562 J.: Calculation of the sensitivity of proton-transfer-reaction mass spectrometry (PTR-
563 MS) for organic trace gases using molecular properties, *International Journal of Mass
564 Spectrometry*, 421, 71-94, 10.1016/j.ijms.2017.04.006, 2017.
- 565 Sheehy, P. M., Volkamer, R., Molina, L. T., and Molina, M. J.: Oxidative capacity of
566 the Mexico City atmosphere - Part 2: A ROx radical cycling perspective, *Atmospheric
567 Chemistry and Physics*, 10, 6993-7008, 10.5194/acp-10-6993-2010, 2010.
- 568 Sinha, V., Williams, J., Crowley, J. N., and Lelieveld, J.: The Comparative Reactivity
569 Method – a new tool to measure total OH Reactivity in ambient air, *Atmos.
570 Chem. Phys.*, 8, 2213-2227, 10.5194/acp-8-2213-2008, 2008.
- 571 Stone, D., Whalley, L. K., and Heard, D. E.: Tropospheric OH and HO₂ radicals: field
572 measurements and model comparisons, *Chem. Soc. Rev.*, 41, 6348-6404,
573 10.1039/c2cs35140d, 2012.
- 574 Tan, Z., Fuchs, H., Lu, K., Hofzumahaus, A., Bohn, B., Broch, S., Dong, H., Gomm, S.,
575 Häsel, R., He, L., Holland, F., Li, X., Liu, Y., Lu, S., Rohrer, F., Shao, M., Wang, B.,
576 Wang, M., Wu, Y., Zeng, L., Zhang, Y., Wahner, A., and Zhang, Y.: Radical chemistry
577 at a rural site (Wangdu) in the North China Plain: observation and model calculations



- 578 of OH, HO₂ and RO₂ radicals, *Atmos. Chem. Phys.*, 17, 663-690, 10.5194/acp-17-663-
579 2017, 2017.
- 580 Tan, Z., Rohrer, F., Lu, K., Ma, X., Bohn, B., Broch, S., Dong, H., Fuchs, H., Gkatzelis,
581 G. I., Hofzumahaus, A., Holland, F., Li, X., Liu, Y., Liu, Y., Novelli, A., Shao, M., Wang,
582 H., Wu, Y., Zeng, L., Hu, M., Kiendler-Scharr, A., Wahner, A., and Zhang, Y.:
583 Wintertime photochemistry in Beijing: observations of RO_x radical concentrations in
584 the North China Plain during the BEST-ONE campaign, *Atmos. Chem. Phys.*, 18,
585 12391-12411, 10.5194/acp-18-12391-2018, 2018.
- 586 Tan, Z., Lu, K., Hofzumahaus, A., Fuchs, H., Bohn, B., Holland, F., Liu, Y., Rohrer, F.,
587 Shao, M., and Sun, K.: Experimental budgets of OH, HO₂, and RO₂ radicals and
588 implications for ozone formation in the Pearl River Delta in China 2014, *Atmospheric
589 chemistry and physics*, 19, 7129-7150, 2019a.
- 590 Tan, Z., Lu, K., Jiang, M., Su, R., Wang, H., Lou, S., Fu, Q., Zhai, C., Tan, Q., Yue, D.,
591 Chen, D., Wang, Z., Xie, S., Zeng, L., and Zhang, Y.: Daytime atmospheric oxidation
592 capacity in four Chinese megacities during the photochemically polluted season: a case
593 study based on box model simulation, *Atmos. Chem. Phys.*, 19, 3493-3513,
594 10.5194/acp-19-3493-2019, 2019b.
- 595 Tan, Z. F., Lu, K. D., Hofzumahaus, A., Fuchs, H., Bohn, B., Holland, F., Liu, Y. H.,
596 Rohrer, F., Shao, M., Sun, K., Wu, Y. S., Zeng, L. M., Zhang, Y. S., Zou, Q., Kiendler-
597 Scharr, A., Wahner, A., and Zhang, Y. H.: Experimental budgets of OH, HO₂, and RO₂
598 radicals and implications for ozone formation in the Pearl River Delta in China 2014,
599 *Atmospheric Chemistry and Physics*, 19, 7129-7150, 10.5194/acp-19-7129-2019,
600 2019c.
- 601 Tonnesen, G. S., and Dennis, R. L.: Analysis of radical propagation efficiency to assess
602 ozone sensitivity to hydrocarbons and NO_x: 1. Local indicators of instantaneous odd
603 oxygen production sensitivity, *Journal of Geophysical Research: Atmospheres*, 105,
604 9213-9225, 2000.
- 605 Volkamer, R., Sheehy, P., Molina, L. T., and Molina, M. J.: Oxidative capacity of the
606 Mexico City atmosphere - Part 1: A radical source perspective, *Atmospheric Chemistry
607 and Physics*, 10, 6969-6991, 10.5194/acp-10-6969-2010, 2010.
- 608 Wang, C., Yuan, B., Wu, C., Wang, S., Qi, J., Wang, B., Wang, Z., Hu, W., Chen, W.,
609 Ye, C., Wang, W., Sun, Y., Wang, C., Huang, S., Song, W., Wang, X., Yang, S., Zhang,
610 S., Xu, W., Ma, N., Zhang, Z., Jiang, B., Su, H., Cheng, Y., Wang, X., and Shao, M.:
611 Measurements of higher alkanes using NO⁺ chemical ionization in PTR-ToF-MS:
612 important contributions of higher alkanes to secondary organic aerosols in China,
613 *Atmospheric Chemistry and Physics*, 20, 14123-14138, 10.5194/acp-20-14123-2020,
614 2020a.
- 615 Wang, W., Parrish, D. D. P., Li, X., Shao, M., Liu, Y., Lu, S., Hu, M., Wu, Y., Zeng, L.,
616 and Zhang, Y.: Exploring the drivers of the elevated ozone production in Beijing in
617 summertime during 2005–2016, *Atmospheric Chemistry and Physics Discussions*, 1-
618 40, 2020b.
- 619 Wang, W., Qi, J., Zhou, J., Yuan, B., Peng, Y., Wang, S., Yang, S., Williams, J., Sinha,
620 V., and Shao, M.: The improved comparative reactivity method (ICRM): measurements
621 of OH reactivity under high-NO_x conditions in ambient air, *Atmos. Meas. Tech.*, 14,



622 2285-2298, 2021.
623 Womack, C. C., McDuffie, E. E., Edwards, P. M., Bares, R., de Gouw, J. A., Docherty,
624 K. S., Dubé, W. P., Fibiger, D. L., Franchin, A., Gilman, J. B., Goldberger, L., Lee, B.
625 H., Lin, J. C., Long, R., Middlebrook, A. M., Millet, D. B., Moravek, A., Murphy, J. G.,
626 Quinn, P. K., Riedel, T. P., Roberts, J. M., Thornton, J. A., Valin, L. C., Veres, P. R.,
627 Whitehill, A. R., Wild, R. J., Warneke, C., Yuan, B., Baasandorj, M., and Brown, S. S.:
628 An Odd Oxygen Framework for Wintertime Ammonium Nitrate Aerosol Pollution in
629 Urban Areas: NO_x and VOC Control as Mitigation Strategies, *Geophys. Res. Lett.*, 46,
630 4971-4979, 10.1029/2019gl082028, 2019.
631 Wu, C., Wang, C., Wang, S., Wang, W., Yuan, B., Qi, J., Wang, B., Wang, H., Wang, C.,
632 Song, W., Wang, X., Hu, W., Lou, S., Ye, C., Peng, Y., Wang, Z., Huangfu, Y., Xie, Y.,
633 Zhu, M., Zheng, J., Wang, X., Jiang, B., Zhang, Z., and Shao, M.: Measurement report:
634 Important contributions of oxygenated compounds to emissions and chemistry of
635 volatile organic compounds in urban air, *Atmospheric Chemistry and Physics*, 20,
636 14769-14785, 10.5194/acp-20-14769-2020, 2020.
637 Ye, C., Yuan, B., Lin, Y., Wang, Z., Hu, W., Li, T., Chen, W., Wu, C., Wang, C., Huang,
638 S., Qi, J., Wang, B., Wang, C., Song, W., Wang, X., Zheng, E., Krechmer, J. E., Ye, P.,
639 Zhang, Z., Wang, X., Worsnop, D. R., and Shao, M.: Chemical characterization of
640 oxygenated organic compounds in the gas phase and particle phase using iodide CIMS
641 with FIGAERO in urban air, *Atmospheric Chemistry and Physics*, 21, 8455-8478,
642 10.5194/acp-21-8455-2021, 2021.
643 Yu, Y., Cheng, P., Li, H., Yang, W., Han, B., Song, W., Hu, W., Wang, X., Yuan, B.,
644 Shao, M., Huang, Z., Li, Z., Zheng, J., Wang, H., and Yu, X.: Budget of nitrous acid
645 (HONO) and its impacts on atmospheric oxidation capacity at an urban site in the fall
646 season of Guangzhou, China, *Atmos. Chem. Phys. Discuss.*, 2021, 1-38, 10.5194/acp-
647 2021-178, 2021.
648 Yuan, B., Liggio, J., Wentzell, J., Li, S. M., Stark, H., Roberts, J. M., Gilman, J., Lerner,
649 B., Warneke, C., Li, R., Leithead, A., Osthoff, H. D., Wild, R., Brown, S. S., and de
650 Gouw, J. A.: Secondary formation of nitrated phenols: insights from observations
651 during the Uintah Basin Winter Ozone Study (UBWOS) 2014, *Atmos. Chem. Phys.*, 16,
652 2139-2153, 10.5194/acp-16-2139-2016, 2016.
653 Yuan, B., Koss, A. R., Warneke, C., Coggon, M., Sekimoto, K., and de Gouw, J. A.:
654 Proton-Transfer-Reaction Mass Spectrometry: Applications in Atmospheric Sciences,
655 *Chem. Rev.*, 117, 13187-13229, 10.1021/acs.chemrev.7b00325, 2017.
656
657
658
659

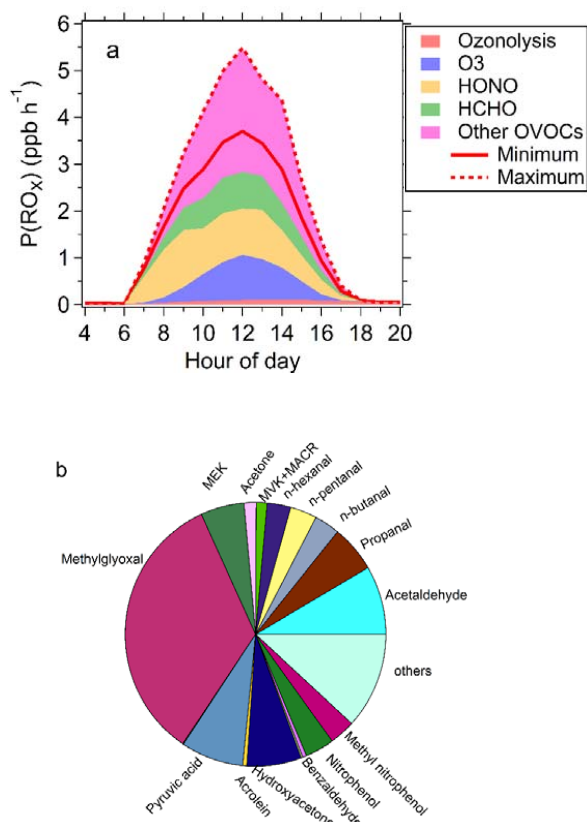


660

661 Figure 1. The average diurnal variations of the concentrations of photodegradable
662 OVOCS species during the field campaign in Guangzhou.

663

664



665

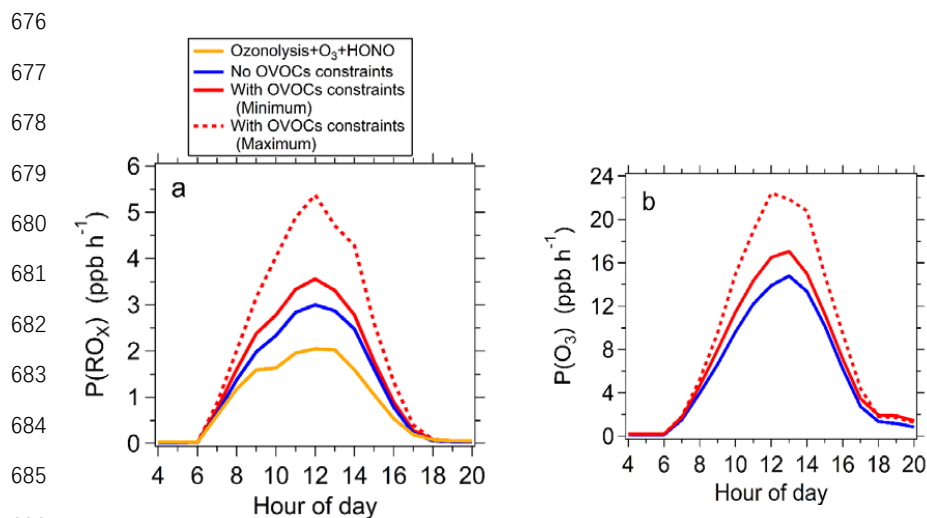
666

667 Figure 2. The P(RO_x) calculated by box model with all observed photodegradable
668 species constrained. (a): The source composition of total P(RO_x) during the campaign;
669 the solid and dashed lines represent the scenarios with minimum and maximum OVOC
670 contributions to P(RO_x), respectively. (b): the relative contributions of non-HCHO
671 OVOC species to P(RO_x) for the scenarios with minimum OVOC contribution to
672 P(RO_x).

673

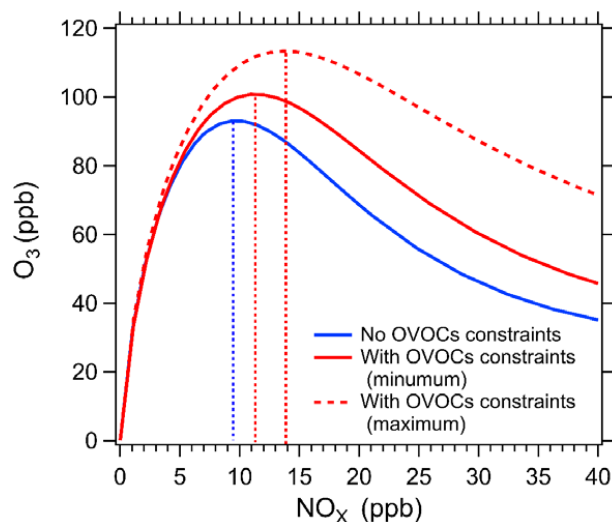
674

675



687 Figure 3. Model simulated P(RO_x) (a) and P(O₃) (b) without and with all observed
688 photodegradable OVOCs constrained. (a): Model simulated P(RO_x) without (blue line)
689 and with all observed photodegradable OVOCs constrained (red lines). The sum
690 contribution of O₃ photolysis, HONO photolysis and ozonolysis is also displayed
691 (yellow line). (b): Model simulated P(O₃) without (blue line) and with observed
692 photodegradable OVOCs constrained (red lines). The red solid and red dashed lines
693 represent the scenarios with minimum and maximum OVOC contributions to P(RO_x),
694 respectively.

695
696
697



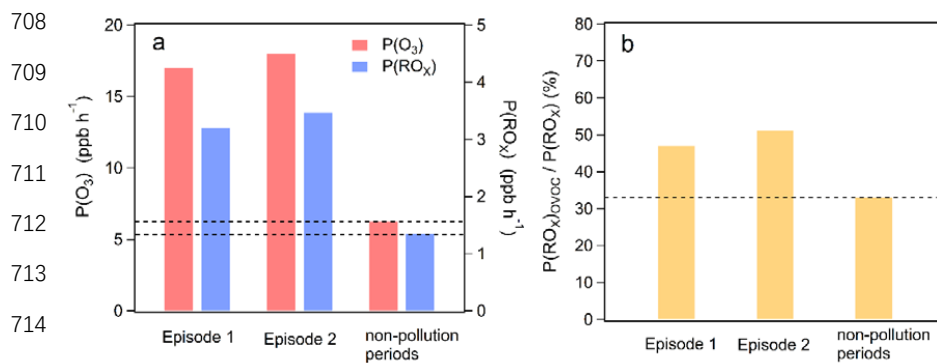
698

699 Figure 4. Model simulated dependence of daily peak O₃ concentrations on NO_x
700 concentrations without (blue curve) and with all observed photodegradable OVOCs
701 constrained (red curves). The red solid and red dashed curves represent the scenarios
702 with minimum and maximum OVOC contributions to P(RO_x), respectively. The dashed
703 lines parallel to Y-axis represent the threshold of NO_x levels to distinguish between
704 VOC-limited and NO_x-limited regimes.

705

706

707



716 Figure 5. Averaged $P(O_3)$, $P(RO_x)$, the ratio of $P(RO_x)$ contributed by OVOCs to total
717 $P(RO_x)$ ($P(RO_x)_{OVOC}/P(RO_x)$) during two ozone pollution episodes (episode 1,
718 episode 2) and non-pollution periods. Both $P(O_3)$ and $P(RO_x)$ correspond to the
719 scenarios with minimum OVOC contributions to $P(RO_x)$.

720

721

722